

ARTICLE

Open Access



A Sarcocystidae-Specific striated fiber assemblin protein SFA5 is required for parasite division in *Toxoplasma gondii*

Yuebao Li^{1†}, Xiaoyan Tang^{1†}, Kai He^{1†}, Hui Dong¹, Hui-Yong Ding¹, Xi-Ting Wu¹, Xiao-Wei Chen¹, Rui-Bin Wu¹, Qiang-Qiang Wang¹, Muhammad Tahir Aleem² and Shaojun Long^{1*} 

Abstract

Apicomplexan encompass a variety of intracellular parasites responsible for significant diseases in humans and animals, such as malaria and toxoplasmosis. Among these, *Toxoplasma gondii* (*T. gondii*) serves as an exemplary organism for understanding the intricate biological characteristics of the phylum. At the parasite's apical tip, a striated fiber was discovered and proposed to be evolutionarily derived from the algal flagellum. However, the protein composition (the striated fiber assemblin, SFA) of this fiber remains poorly understood. Here, we took advantage of a proximity biotiny labeling approach to identify potential SFA proteins by fusion of an engineered biotiny ligase TurboID with SFA2, from which we identified several novel components of the fiber. Evolutionary analysis suggested that SFA4 is conserved in the Apicomplexa phylum with the exception of piroplasmida, while SFA5 is specific to species of Sarcocystidae. Confocal imaging analysis showed that SFA4 and SFA5 are substantially co-localized with the bait SFA2. Using a new version (OsTIR1^{F74G}) of the plant auxin-inducible degron system that we adapted in this study, we found that SFA4 and SFA5 were efficiently depleted by addition of a much lower concentration of inducer (5-Ph-IAA, instead of IAA). Detailed phenotypical analyses demonstrated that SFA5 is essential for daughter parasite formation and separation of parasite nuclei during division, supporting the localization of SFA5 at the striated fiber that connects the centriole and the apical conoid. The mouse assay suggested the essentiality of SFA5 in the parasites. Thus, this study provided a new repertoire of the striated fiber, and new data supporting association of the fiber with parasite division.

Keywords *Toxoplasma gondii*, Striated fiber assemblin, Protein components, Plant auxin inducible degron system, Parasite division

Introduction

The phylum Apicomplexa contains over 5000 parasites, the majority of which are intracellular. *Toxoplasma gondii*, the phylum's most successful model species, is capable of infecting nearly all warm-blooded creatures, including humans, and possesses genetic adaptability within cell cultures. After invading into host cell, *T. gondii* resides within a parasitophorous vacuole (PV) in host cells, and then undergoes a complex developmental processes including replication, division and assembly of new daughter zoites. The dynamic and repeated cycle of *T. gondii* can cause widespread infection in intermediate

[†]Yuebao Li, Xiaoyan Tang and Kai He contributed equally to this work.

*Correspondence:

Shaojun Long
LongS2018@163.com

¹ National Key Laboratory of Veterinary Public Health and Safety, College of Veterinary Medicine, China Agricultural University, Beijing 100193, China

² Center for Gene Regulation in Health and Disease, Department of Biological, Geological, and Environmental Sciences, College of Sciences and Health Professions, Cleveland State University, Cleveland, OH 44115, USA



hosts and acute toxoplasmosis in immunocompromised individuals such as HIV-infected people or pregnant women [1, 2]. Of interest is that all severity and pathology of toxoplasmosis originates from tissue destruction caused by the rapid replication cycle of the parasites and by lytic cycle in host cells. In this process, the parasite replication mechanism plays a core role in the maintenance of invasion capability [3–5].

Intracellular cell division of *T. gondii* has attracted attention from the research community over the past few decades [6]. The parasite exhibits the ability to utilize a variety of division strategies, adapting to the environment of the host cell, making it significantly different from the standard eukaryotic division apparatus [7, 8]. Briefly, in the tissues of intermediate hosts, parasite division depends on internal budding or endodyogeny, whereas in the intestinal epithelium of the cat, the parasite undergoes schizogony [9]. So far, many division-associated markers have been discovered, which can be used for exploring the complex biology of parasite division in *T. gondii*. For instance, Centrin 1 localizes to the centrosome of both interphase and mitotic cells in the asexual replication cycle, reflecting the dynamic behavior of the centrosome during the division process [10]. After replication of the centrosome, the daughter parasites begin to assemble, which is initiated in close physical proximity to the centrosome and coincides with the synthesis phase (S-phase) in time [11]. Moreover, Inner Membrane Complex (IMC) proteins were reported to link to each other through certain skeletal elements that form seams, lattices or membrane anchors, and have the ability to further expand the microtubule scaffold of the budding daughter cell further expand [12, 13]. Undoubtedly, these discoveries contribute to understanding of the intracellular replication of the parasite.

Apicomplexan parasites are believed to have evolved from photosynthetic flagellated algae but have lost their flagella along the way [14]. In *T. gondii*, the Striated Fiber Assembly (SFA) fiber acts as the rootlet of the flagellar basal bodies, which is essential for cell division [15]. This structure is a microtubule protein fiber that is attached to the conoid, a motile cone-shaped structure that is part of the apical complex in *T. gondii* [16]. Interestingly, following the centrosome replication, the fiber emerges and elongates away from the centrosome, and eventually attaches the distal end to the conoid microtubule organizing center (MTOC) of the daughter cell [15]. A previous study identified two SFA proteins, namely SFA2 and SFA3 that are homologous proteins of algal flagellum components. This study proposed that the proteins serve as spatial and temporal organizers for the division process of *T. gondii*. The ablation of either SFA2 or SFA3 renders the fibroid structure defective and blocks the

budding of the daughter cell [15]. Together, these previous pieces of evidence indicate that the SFA fiber physically link the centrosome to the conoid, thereby affecting the parasite division [15, 17].

Despite the essential roles of the SFA fiber in *T. gondii* division, there is still a lack of detailed dissection of the protein composition in the fiber. So far, only three SFA-related proteins (SFA1-3) have been characterized, limiting our understanding of the fiber and its function in the parasite. Here, we took advantage of the engineered biotin proximity labeling technique to exploit the protein composition of the striated fiber, from which several novel SFA proteins, SFA4 and SFA5, were discovered. By applying a new version of the plant auxin-inducible degron system (TIR1^{F74G}) that we adapted in this study, our detailed phenotype analyses revealed that the Sarcocystidae-Specific SFA5 is required for the formation of daughter parasite. This study provided a new repertoire of the striated fiber, including an essential protein SFA5, supporting the association of the SFA fiber with parasite division in *T. gondii* and potentially in other related protists.

Results

Construction of SFA2-TurboID for proximal biotin labeling in *T. gondii*

To examine the intricate protein interaction and identification of novel proteins in the SFA fiber, a biotin proximity protein labeling approach was used. The latest version of biotin ligase TurboID was endogenously tagged at the C terminus of SFA2 using the CRISPR tagging approach recently introduced in *T. gondii* [18] (Fig. 1A). Immunofluorescence assays (IFA) were performed on the SFA2 transgenic parasites, confirming the successful fusion of the TurboID-4Ty tag with SFA2 (Fig. 1B). Western blot assay using the Ty monoclonal antibody exhibited a single band of protein with the correct size for SFA2-TurboID-4Ty (Fig. 1B). To examine the biotin labeling activity of the TurboID fusion, IFA was performed with a streptavidin reagent for parasites treated with and without biotin, revealing additional spots that are co-localized with the TurboID fusion protein in the parasites of SFA2-TurboID-4Ty (Fig. 1C). Collectively, the TurboID fusion was successfully generated and able to label proximal proteins in the parasites for further experiments.

SFA4 and SFA5 are the novel components of the SFA fiber

To screen candidate proteins, proteomic analysis was performed for the parental line RH Δ ku80 Δ hxgprt and the TurboID fusion line. The spectra data were preliminarily processed using the Scaffold4 software, and a volcano map was plotted to gain the overall distribution of all candidate proteins identified by the proximal biotin

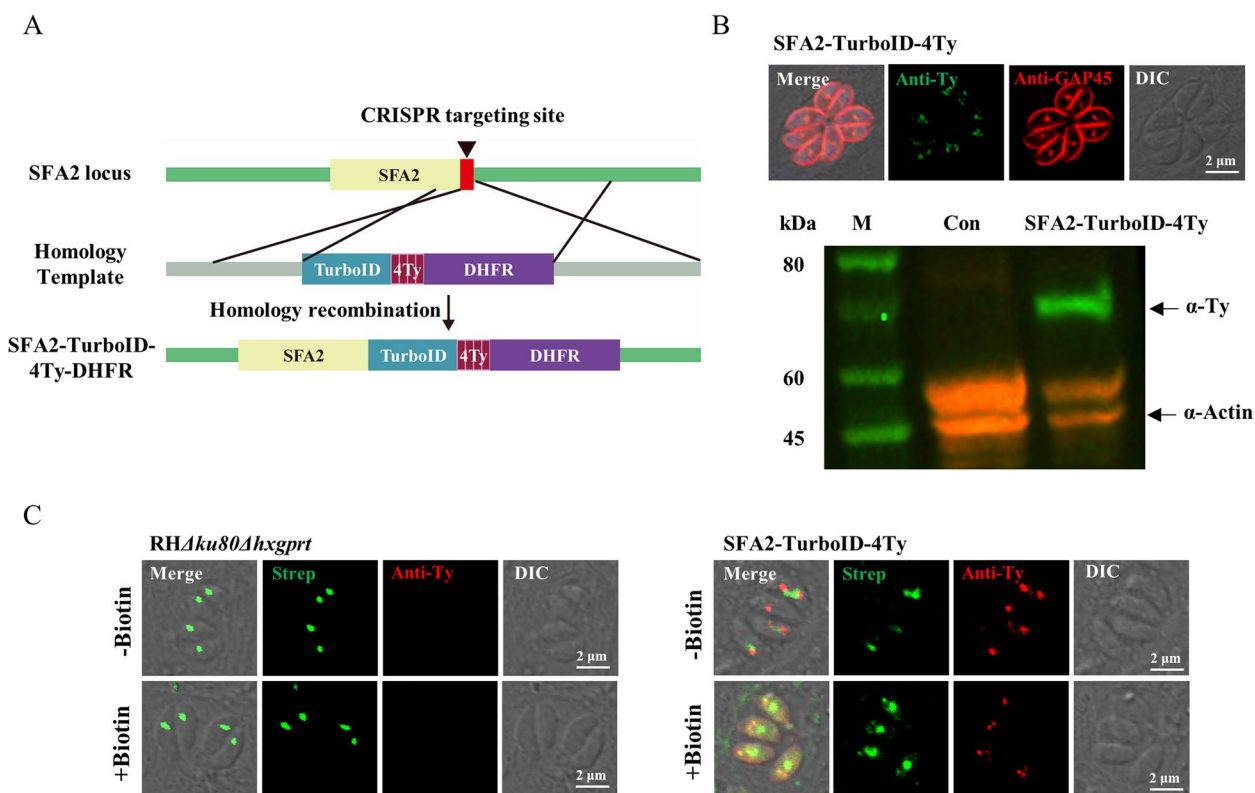


Fig. 1 Construction of SFA2-TurboID in *T. gondii*. **A** Schematic of the CRISPR/Cas9 system used to insert the TurboID-4Ty-DHFR at the C-terminus of SFA2. The sgRNA was selected right downstream of the stop codon, and the homologous regions at the amplicon ends were derived from the upstream and downstream of the stop codon and the sgRNA site respectively. **B–C** Confirmation of the SFA2-TurboID fusion line by IFA and Western blots. Parasites were grown in HFF cells, followed by IFA and Western blots for verification of the TurboID line (**B**), while the labeling activity of the TurboID in the parasites were performed by staining of biotylated proteins using streptavidin Fluor-488 (green) for parasites grown in the presence (+) or absence (-) of biotin (1.5 h) (**C**). Antibodies against Ty (red) and GAP45 (red) were used in the IFA, while Ty stained green was used in Western blot. Scale bar = 2 μ m. Actin served as the control in Western blot. Scale bar = 2 μ m

labeling approach (Fig. 2A) (Table S1). This analysis identified 96 proteins that have higher numbers of spectra in SFA2-TurboID compared to the parental line. Based on the fold change and phenotypic score (Table S1), we attempted to analyze five of the hypothetical proteins with higher numbers of spectra, predicted to be essential to the parasites by referring to the data on ToxoDB

(Fig. 2B). To examine whether these candidate proteins are co-localized with SFA2, CRISPR/Cas9-mediated targeting and homologous recombination were designed to fuse 6xHA with the C-termini of these candidates in the background line of SFA2-6Ty (Fig. S1A). IFA imaging analysis was applied to identify the target proteins in the genetically engineered parasites, which showed that

(See figure on next page.)

Fig. 2 Identification of candidate proteins labeled by TurboID (**A**). The volcano map showing the identified proteins by proximal biotin labeling strategy. The red dots represented significantly up-regulated proteins by comparison with the parental RH line. Five of the candidate proteins for subsequent analysis were labelled in the plot (See Table S1). **B** The candidate proteins were analyzed based on ToxoDB and InterPro databases. **C** Localization of SFA4-6HA (green) and SFA5-6HA (green) in the background parasite line SFA2-6Ty. The HA fusion was stained green while the SFA2Ty was stained red as a reference. The Pearson Correlation coefficient (PCC) was analyzed with $\text{mean} \pm \text{SEM}$ using the intensities over the white line using the NIS software. Three independent experiments were performed with similar outcomes, and The PCC shown were averages and standard deviation ($N=20$). Scale bar = 2 μ m. **D** The model pattern of SFA2 and two novel SFA proteins in *T. gondii*. The segmented Coiled Coil Domain are conserved and drawn as yellow boxes. **E** Robust Multi-array Average (RMA) values of transcripts encoding SFA2 and two novel proteins over two consecutive division cycles based on previous published data from Behnke and co-workers [19]. **F** Parasites expressing SFA2-6Ty and SFA5-6HA were scored by IFA using anti-Ty and anti-HA antibodies in an asynchronous parasite population ($n=200$) for parasites grown in HFF cells for 24 h. The data of image were calculated based on two independent experiments. Error bars represent the standard error

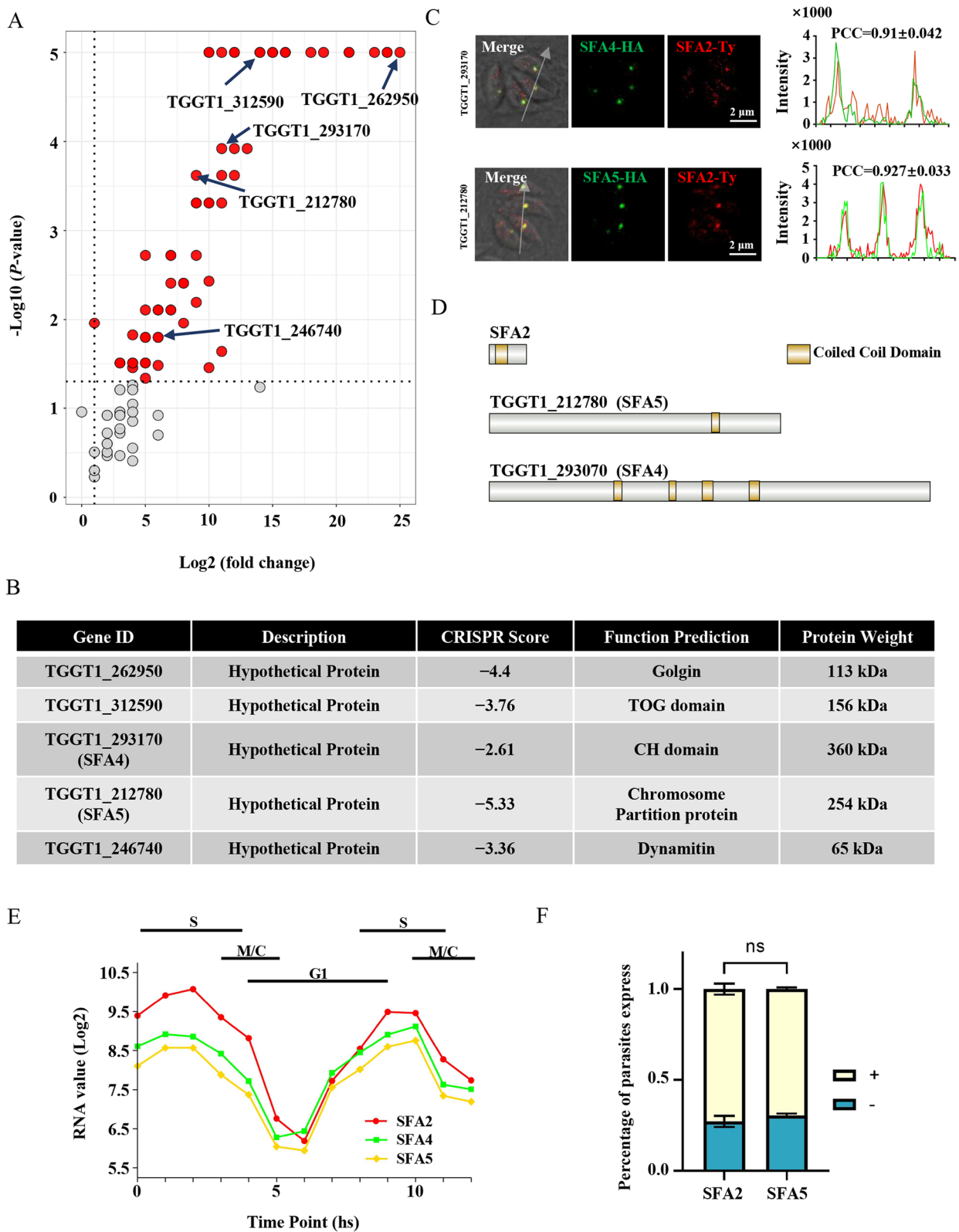


Fig. 2 (See legend on previous page.)

TGGT1_293170 (SFA4), TGGT1_212780 (SFA5) and TGGT1_246740 were substantially co-localized with the bait protein SFA2 (Fig. 2C and Fig. S1B). The co-localization of proteins with SFA2 was further supported by overlapping intensity analysis with calculated Pearson correlation coefficients (PCC) (Fig. 2C). Another two candidates were analyzed in parallel, which showed that no co-localization features were observed with SFA2 for TGGT1_312590 and TGGT1_262950 (Fig. S1B).

We then focused on proteins of SFA4 and SFA5 in the parasite by evolutionary and functional analyses. To compare the SFA fiber proteins, we first analyzed the protein domains of SFA2, SFA4 and SFA5 using InterPro, and found that these proteins contain 1–4 coiled-coil domains (Fig. 2D). Interestingly, both of the new proteins SFA4 and SFA5 are large in protein sizes with 254 kDa (SFA5) and 360 kDa (SFA4) (Fig. 2D). A previous study illustrates that the transcription of the SFA2 gene fluctuates according to the cell cycle, with maximal expression aligning with DNA replication and mitosis events [15]. We then compared the expression of genes of SFA4 and SFA5 with that of SFA2, and observed a similar expression feature in the cell cycle (Fig. 2E, F). These features provide additional evidence supportive of the fiber localization of the novel proteins SFA4 and SFA5.

SFA5 is conserved in Sarcocystidae parasites

SFA1-3 were identified in the Apicomplexans, based on the sequence homolog to the proteins in flagella in green algae, although the Apicomplexa lack flagella with the exception of the male gamete produced during the sexual stages in the intestine of cats [10]. We then analyzed the phylogeny of SFA2, SFA4 and SFA5 using jackhammer search of our customized databases. Expectedly, we found that SFA2 is conserved in the chlorophyta (green algal) species and in protists, such as the *ciliates* and *oomycetes* (Fig. S2). Of note, the phylogeny of SFA2 formed a large branch in the tree, which is consistent

with the proposed origin of the SFA fiber structure. Intriguingly, SFA4 is well conserved in the apicomplexan parasites only with the exception of parasites belonging to the piroplasmida, which is depicted by red branches in the tree (Fig. S2). In contrast, SFA5 was identified only in specific species of the Sarcocystidae, such as *Neospora caninum*, *Besnoitia besnoiti* and *Cystoisopora suis* (Fig. S2 and Table S2), which is depicted by green branches in the phylogeny tree (Fig. S2). Taken together, SFA4 and SFA5 are clearly less conserved in comparison with SFA2 in the algae and the Apicomplexa, likely suggesting a difference in protein essentiality in the parasite.

SFA5 is indispensable for parasite growth in vitro

We then determined to dissect the function of SFA4 and SFA5 in the parasite by applying the plant auxin-inducible degron system (AID) [16, 20]. Recently, it was reported that a mutation (F74G) of the auxin receptor TIR1 allowed TIR1 to accept a larger ligand 5-Ph-IAA, and fusion of the miniAID degron with a target protein is able to deplete the target very efficiently by the system [21]. We attempted to adapt the system in the parasite prior to the function dissection of the novel proteins, by expression of the mutated copy (F74G) of the TIR1, as demonstrated in Fig. 3A. The gene loci of SFA4 and SFA5 were fused with miniAID in the parental line TIR1^{F74G}, using a CRISPR tagging approach (Fig. 3C), as described in our previous study [16]. The engineered mAID tags at the C-termini of SFA4 and SFA5 were examined by IFA, which showed that the fusions of SFA4 and SFA5 were expectedly localized to the spot at the anterior of the parasites (Fig. 3D). Addition of the ligand 5-Ph-IAA (working concentration at 2 μ M) efficiently depleted the protein level of SFA4 and SFA5 after 12 h of induction, as demonstrated by the IFA and Western blot (Fig. 3D). The induction efficiency, as demonstrated by the fusion of SFA4 and SFA5, suggested that the new version of AID

(See figure on next page.)

Fig. 3 Construction and characterization of conditional knockdown lines SFA4-mAID and SFA5-mAID **(A)** mutation of DNA sequences encoding position 74 at the TIR1. The DNA sequence of TIR1 encoding the 74th amino acid was sequenced and shown was the mutation site. **B** the new version of TIR1-Flag was expressed in the parasite to generate a parental line TIR1^{F74G}. **C** Schematic of the CRISPR/Cas9 system used for inserting the mAID-6Ty-DHFR at the C-terminus of the SFA4 or SFA5. The pCas9-sgRNA (that encodes a sgRNA targeting to the downstream of the stop codon) and amplicon (that contains homologous regions and the mAID-6Ty-DHFR) were transfected into the TIR1^{F74G} line, resulting in the mAID-6Ty-DHFR fragments fusing at the C-terminus of SFA4 or SFA5. Note that DHFR indicates the resistant expression cassette. **D–E** Immunofluorescence microscopy and Western blot of SFA4-mAID-Ty and SFA5-mAID-Ty lines grown with/without 5-Ph-IAA treatment for 16 h. The parasites were stained using mouse anti-Ty (SFA4 for green, SFA5 for red) and rabbit anti-GAP45 (the SFA4-mAID line for red, the SFA5-mAID line for green). Scale bar = 2 μ m. SFA4-mAID-6Ty and SFA5-mAID-6Ty tachyzoites were grown on HFF with/without 5-Ph-IAA treatment for 16 h. Labels were detected by mouse anti-Ty and rabbit anti-Actin (or Tubulin) as control. **F–G** Plaque formation with TIR1, SFA4-mAID and SFA5-mAID lines grown with/without 5-Ph-IAA for 7 days. The numbers of plaques were scored using ImageJ. Three independent experiments were performed. ****, $p < 0.0001$. **H** Parasites were grown in HFF cells in treatment (+ 5-Ph-IAA) or control (ethanol) for 24 h. IFA was performed for scoring vacuoles containing different numbers of parasites. Means \pm SEM of three biological replicates with Two-way ANOVA analysis. ***, $p < 0.001$

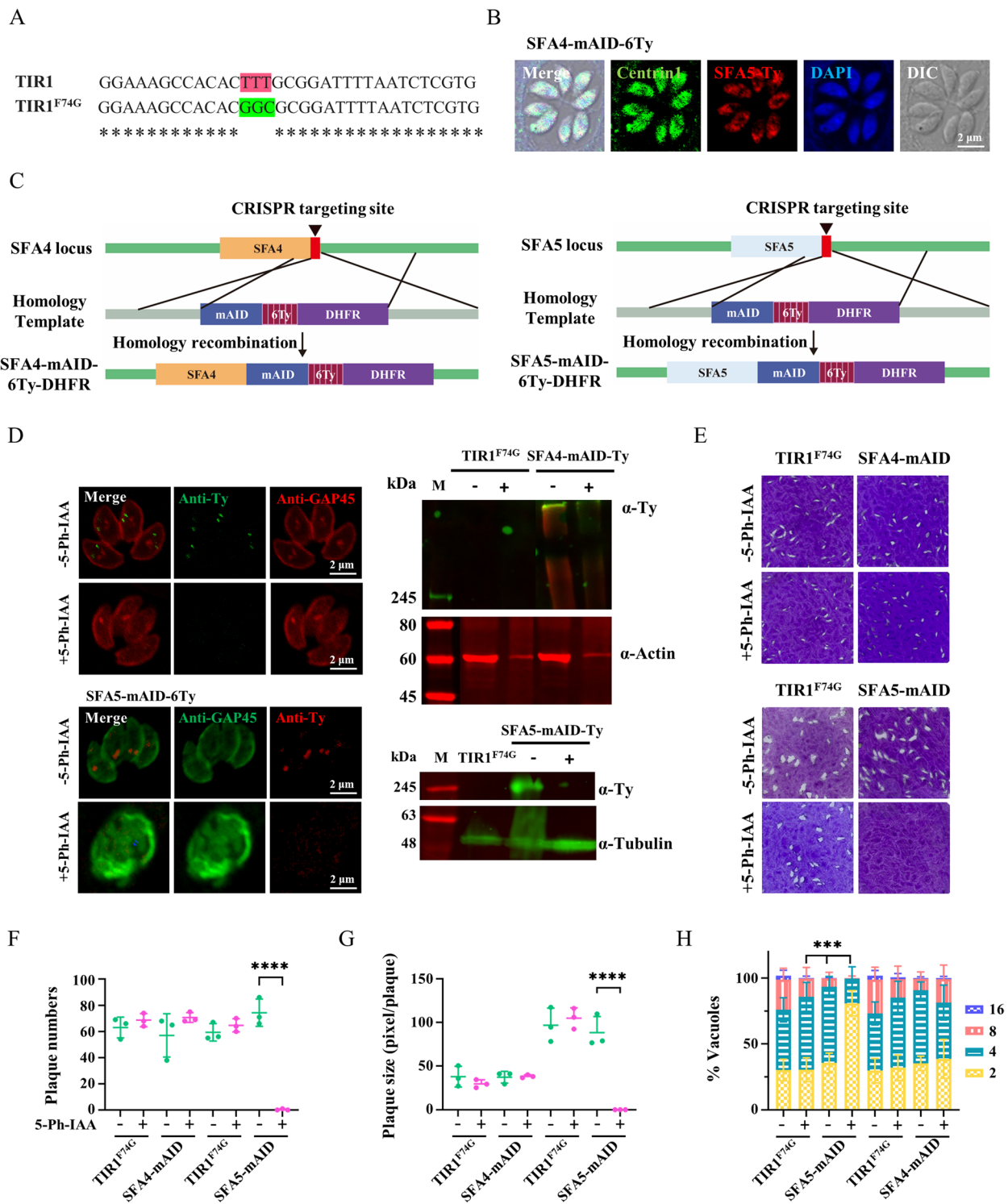


Fig. 3 (See legend on previous page.)

system (TIR1^{F74G}) is efficient in depletion of target fusion proteins, using a much lower ligand 5-Ph-IAA.

These IFA results provided the first observation of the parasites depleted with SFA4 and SFA5, which showed

that depletion of SFA4 had no apparent defects in parasite morphology, while depletion of SFA5 caused an abnormal localization of GAP45 and distorted parasite morphology (Fig. 3D). To evaluate the importance

of mAID fusions for parasite proliferation, we analyzed their capacity to form plaques on host cells during the parasite's lytic cycle. Notably, the SFA5-mAID parasite line, when cultivated in the presence of 5-Ph-IAA, formed no visible plaques. In contrast, the SFA4-mAID line exhibited normal growth (Fig. 3E). These results were further supported by scoring of plaque numbers with the SFA fusion lines (Fig. 3F, G), suggesting that SFA5 is essential for parasite growth in host cells. To determine whether the protein depletions have effects on parasite replication, we assayed the parasite numbers in single vacuoles in the lines grown with or without the inducer 5-Ph-IAA (2 μ M). The SFA5-mAID line had a clear defect on parasite replication, as judged by much fewer vacuoles with 16 and 8 parasites per vacuole, and the accumulation of low numbers of parasites per vacuoles (Fig. 3H). In contrast, the SFA4-mAID line had no obvious effect on the parasite replication

(Fig. 3H). Collectively, we adapted a new version of plant auxin-inducible degron system (TIR1^{F74G}), by which we identified SFA5 as an essential component of the striated fiber in the parasite.

SFA5 is involved in formation of daughter parasites

To examine the morphology of parasites depleted with SFA5, we employed a variety of *T. gondii* organelle markers to observe changes in the parasite morphology following depletion of SFA5 by addition of the ligand. We tested formation and separation of the centriole by staining the parasites with Centrin 1, parasite morphology by staining of the IMC markers IMC1, GAP45, and MLC1, organelle status by staining markers ACP and Bip, and the parasite cytoskeleton by staining tubulin. In the parasites without treatment with 5-Ph-IAA, we observed that all the staining of markers were localized to the expected locations, and the differential interference contrast

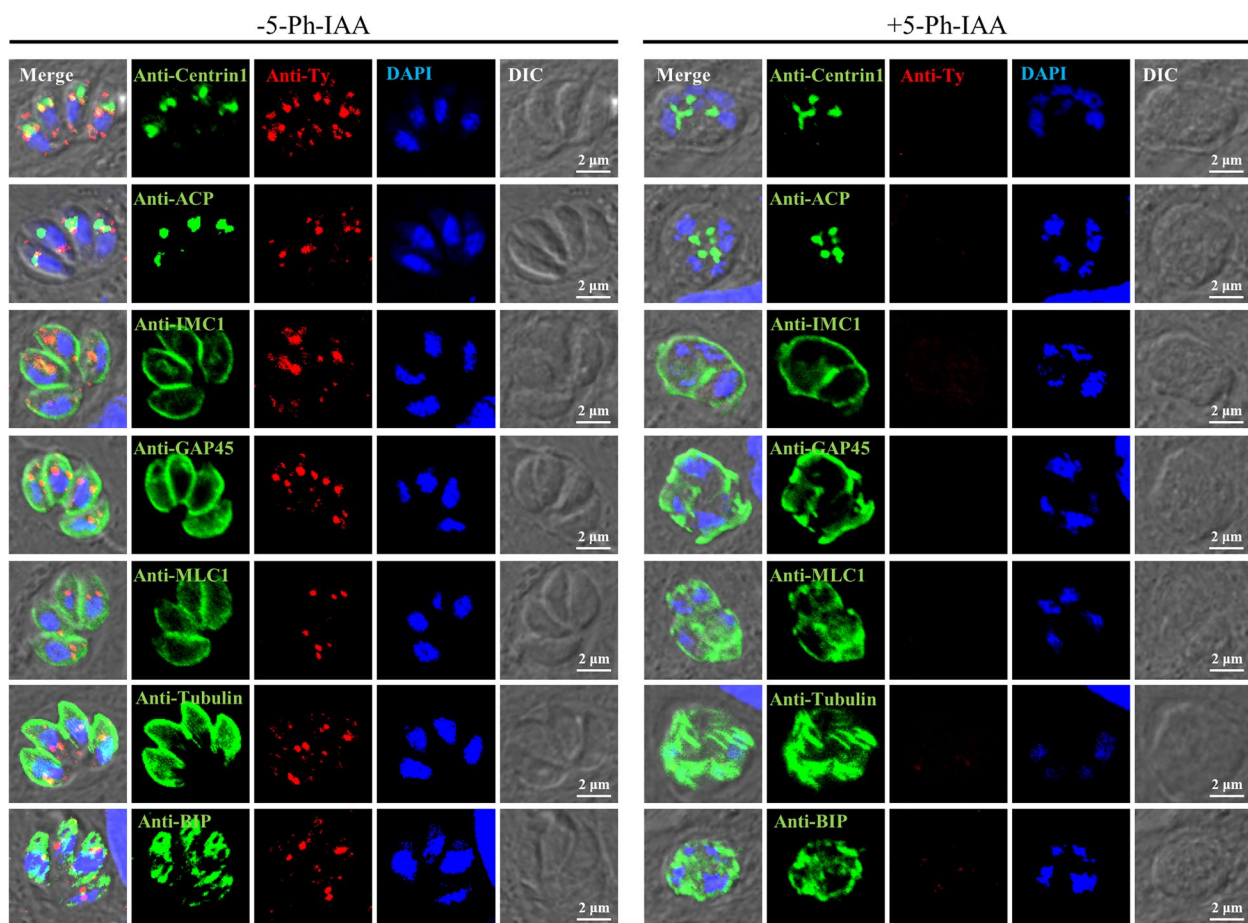


Fig. 4 Parasites depleted with SFA5 show pronounced phenotypic defects. Parasites of SFA5-mAID were grown in presence (+) or absence (-) of 5-Ph-IAA for 16 h, followed by IFA analysis using antibodies against markers (green) for the centriole (centrin1), the apicoplast (ACP), the endoplasmic reticulum (Bip), the cytoskeleton tubulin and the inner membrane complex (GAP45, IMC1 and MLC1). The mAID-Ty fusion was labelled with red to show the presence or the absence of the fusion protein. Three independent experiments were performed with similar outcomes, and scale bar = 2 μ m

(DIC) clearly showed individual parasites in vacuoles (Fig. 4). In deep contrast, in the mAID fusion parasites grown in the ligand for 16 h, we observed a spherical parasite body (Fig. 4), while the IMC stainings failed to clearly identify individual parasites within the parasite bodies (Fig. 4). Furthermore, in the spherical parasites, we observed multiple stainings of centrin1, ACP, and nucleus, each centrin1 and ACP stainings coupled with a nucleus staining. In addition, depletion of SFA5 obviously disrupted the organization of the tubulin cytoskeleton and the endoplasmic reticulum marker Bip (Fig. 4). These results collectively suggested that the parasites depleted with SFA5 were able to duplicate the organelles, however, they were unable to properly form daughter parasites, resulting in distorted parasites and enlarged parasite body.

SFA5 is essential for parasite virulence of *Toxoplasma* in mice

To investigate the roles of SFA5 in the virulence of tachyzoites, intraperitoneal infection was conducted in mice with 100 tachyzoites of the TIR1^{F74G} parental line and the SFA5-mAID parasites. The control mice were administered with a solution without the inducer 5-Ph-IAA, while the experimental group was supplied with a solution containing 5-Ph-IAA on a daily basis. The mouse survival assay showed that all mice in the control group (with TIR1^{F74G} parental line and SFA5-AID) without 5-Ph-IAA died on day 8–10, while mice infected with SFA5-mAID and treated with 5-Ph-IAA survived (Fig. 5A). Conversely, the mice infected with the TIR1^{F74G} parental line but treated with 5-Ph-IAA clearly survived, further supporting that depletion of SFA5 had a

lethal effect on parasite survival in vivo. Meanwhile, the body weight of all mice were monitored daily, which showed that the mice infected with SFA5-mAID and supplied with 5-Ph-IAA appeared to be normal, while mice in the control groups began to lose body weight on day 5 (Fig. 5B). In summary, SFA5 is essential for parasite growth in mice, suggesting that the association of SFA5 with the fiber is critical for parasite growth.

Discussion

Parasite division utilizes the positioning and assembly of a fiber evolutionarily derived from an algal flagellum [15]. This fiber comprises homologs of the proteins found in striated fiber assemblins, which serve as the principal cytoskeletal component of the striated microtubule-associated fibers (SMAF) located in the flagellar basal apparatus [22–24]. In 2012, Francia and co-workers identified SFA2 and SFA3 as the master regulators in the *T. gondii* cell division [15]. Depletion of SFA2 or SFA3 resulted in defects in daughter cell budding, suggesting the profound role of the proteins in cell division. However, the protein composition of this important fiber remains to be explored, the progress of which could provide further evidence in the fiber functions and evolution in the apicomplexan and evolutionarily related protists. In the past years, knowledge of parasite division in *T. gondii* has expanded, attributing to efficient genetic manipulation tools developed in this model organism of the phylum [25, 26]. In this study, we combined the efficient proximal labeling approach, CRISPR-tagging technology, and the new version of auxin-inducible degradation system (TIR1^{F74G}), to screen and identify novel components of the SFA fiber and to dissect functions of those novel

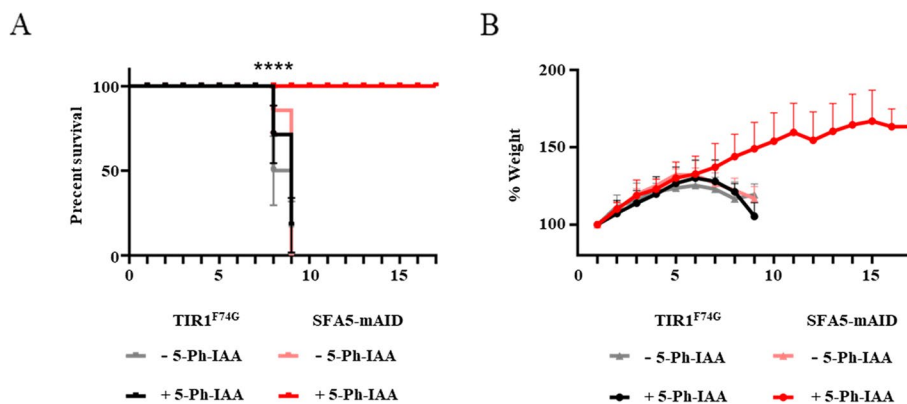


Fig. 5 SFA5 is indispensable during *Toxoplasma* acute infection in mice. **A** Kaplan–Meier curve showing survival of female Balb/c mice with or without *T. gondii* infections. Each mouse was intraperitoneally infected with 100 parasites of TIR1^{F74G} or SFA5-mAID tachyzoites and supplied with water with (+) or without (-) 5-Ph-IAA and with intraperitoneal injection of a solution containing 5-Ph-IAA or PBS on daily basis. Survival data were analyzed by the Gehan-Breslow-Wilcoxon test, comparing to the parental line TIR1^{F74G} without 5-Ph-IAA treatments. **** $p < 0.0001$. **B** Ratio of mouse weight gain after infections with *T. gondii*, as show in (A). The mice were weighted on a daily basis, and the mouse weight on day 0 was considered as the starting point 1. The data were shown with mean \pm SEM

components in the model organism *T. gondii*. Our phenotypic experiments demonstrate that the Sarcocystidae-specific protein SFA5 is essential for formation of daughter parasites in *T. gondii*.

The paired flagella of the algae ancestor were utilized for cell motility and anchored by a cross-shaped system of microtubules and fibrous strands [27, 28]. *Chromalveolate* protists are an important branch of the phylogeny of eukaryotes. A previous report detected a clear spot in *T. gondii* that is close to the centrosome, using SFA antibodies derived from green algae, thus providing a strong evidence supporting the evolutionary relationship between green algae and *T. gondii* in a cellular perspective [10]. SFA, as reported, likely existed in ancestral eukaryotes and was subsequently lost multiple times throughout evolution. Furthermore, despite its broad presence among protists, studies suggest that SFA appears to be absent in multicellular organisms [29]. Thus, it seems possible that *T. gondii* could have conserved certain elements of the flagellar apparatus during its evolutionary process. In our study, we identified additional proteins of the SFA fiber, such as SFA4 and SFA5, which substantially co-localized with SFA2. Additional evidence, which include a common protein domain of coiled-coil and similar expression pattern during cell cycle, further support the localization of the novel proteins at the SFA fiber. However, we noticed that these two proteins have different phylogenetic distribution in the apicomplexan parasites. Except for the parasites of *Babesiidae* and *Theileriidae*, SFA4 homologs are identifiable in the genomes of all other apicomplexan parasites. In contrast, SFA5 is conserved only in the cyst-forming Sarcocystidae parasites. However, it is still noteworthy that the homolog of this protein can not be readily identified in the genomes of other apicomplexans, likely due to the huge size of the protein SFA5. Nevertheless, the conservation of these proteins (i.e., SFA2, SFA4 and SFA5) differs greatly in the apicomplexan parasites.

The SF-assemblins (i.e., SFA1-3) are known to be 269–284 residues of amino acids in length [30]. The discovery of two novel SFA proteins with significantly longer proteins length clearly indicate that the SFA fiber is more complex than expected, as previously thought. Intriguingly, the key SFA proteins contain a coiled-coil domain, which consists of two or more alpha-helices that are twisted together like a rope [29, 31]. This domain is found in many different proteins that have various functions, such as regulating gene expression, forming cytoskeletons, and mediating protein interactions [32–34]. Crucially, evidence illustrates that the coiled coil domain within SFA proteins have the ability to mediate interactions between proteins, thus allowing inter-connection and formation of a fiber with dark striations [10, 35]. In

the regard, it is speculated that there must be more interacting SFA proteins on the fiber structure. Therefore, future studies may be necessary to understand the SFA proteins with emphasis on the molecular structure and biochemical interactions [36, 37].

In recent years, cell division has drawn great attention due to its critical role over in the development lifecycle of *T. gondii* in the host cell. Strikingly, in addition to daughter cell assembly or cytokinesis, DNA replication and nuclear mitosis occur multiple times, which avoids the appearance of the polyploid daughter cells with multiple nuclei [38–40]. Parasites depleted with either SFA2 or SFA3 contained multiple nuclei due to a lack of the SFA fiber, suggesting that the defect was not in mitosis but in the subsequent budding of daughter cells. In our study, cell division was also directly impaired when depleted of SFA5 protein, as observed by the constantly accumulated nucleus and the spherical parasite body. Collectively, the discovery of novel SFA fiber proteins expands our understanding of SFA fiber structure, further recognizing function of the fiber in the parasite division in *T. gondii*, which might be extended to phylogenetically related parasites.

Conclusion

T. gondii division is organized by a homolog of the striated fiber assembling structure evolutionarily derived from green alga. However, so far only three proteins (SFA1-3) have been discovered and characterized. Here we leveraged efficient technologies of TurboID proximity biotinylation and CRISPR genome engineering, discovering 2 novel SFA proteins from a screen of proteomic candidates, namely, SFA4 and SFA5. Within the plant auxin-inducible degradation system, we successfully constructed conditional knockdown strain of SFA4 and SFA5 and accomplish a series of phenotype assay. Notably, although both of SFA4 and SFA5 share common localization and structural features with SFA2, only SFA5 is restricted to Sarcocystida parasites and is required to parasite survival in vitro and in the mouse model.

Materials and methods

Antibodies and chemicals

Primary antibodies such as rabbit and mouse anti-HA were sourced commercially (Thermo-Fisher, #71–5500 and BioLegend, #901501). Other primary antibodies, including rabbit anti-GAP45, rabbit anti-Actin, rabbit anti-IMC1, rabbit anti-Tubulin, rabbit anti-ACP, rabbit anti-Centrin1, and rabbit anti-MLC1 were developed in-house, following methods elucidated in earlier studies [41, 42]. The mouse anti Ty antibodies were generated from a hybridoma line (BB2), generously given by Professor Philippe Bastin. Secondary antibodies with conjugation to Alexa Fluors (either 488 or 568), both anti-mouse

and anti-rabbit, were obtained from Thermo-Fisher Scientific. LI-COR Biotechnology supplied fluorescent reagents conjugated with LI-COR 800 CW. Chemicals such as 2-(5-Phenyl-1H-indol-3-yl)acetic acid (5-Ph-IAA) (Sigma-Aldrich, #SML3574), mycophenolic acid (Sigma-Aldrich, #M3536), 6-xanthine (Sigma-Aldrich, #X4002), and pyrimethamine (Sigma-Aldrich, #46706) were purchased from commercial sources.

Parasites and host cell culture

The previously characterized strains RH Δ ku80 Δ hxgprt and RH Δ ku80 Δ hxgprt/TIR1^{F74G}, herein referred to as RH Δ ku80 Δ hxgprt and TIR1^{F74G} respectively, served as the progenitor strains for the transgenic lines discussed in this article. These original strains and their derived lines (See Table S3 for details) were cultured on HFF-1 cells (ATCC, SCRC-1041) in DMEM (referred to as D5 medium) fortified with 5% heat-treated fetal bovine serum, 2 mM glutamine, and 100 units of penicillin–streptomycin at 37 °C with a controlled environment of 5% CO₂. Both the parasites and HFF-1 cell lines were kept free from mycoplasma, facilitated by the use of the e-Myco plus kit (Intron Biotechnology). The TIR1^{F74G} strain and corresponding mAID lines were cultured in HFF with either 2 μ M 5-Ph-IAA or 0.01% ethanol for the purpose of the phenotypic assay.

Mice

The vivo experiments of *T. gondii* were observed in Balb/C mice that were six weeks old. The mice were kept in filter-top cages under specific pathogen-free (SPF), with the acquisition of sterile water and food. They were randomly grouped into experimental parties ($n=5$ per group), and subjected to an intraperitoneal (i.p.) injection carrying 100 tachyzoites, after which their health was regularly monitored. This daily check included observing their physical appearance, weight, and response levels. The mouse experiments were conducted according to the guidelines and regulations issued by the Veterinary Office of the China Agricultural University (Issue No. AW11402202-2-1).

CAS9 plasmid construction and generation of *Toxoplasma gondii* lines

The pCas9-sgRNA plasmids (Table S4) were employed for gene tagging utilizing the CRISPR/Cas9 method. The sgRNA aiming for a specific area was chosen utilizing the EuPaGDT online prediction software, and the pCas9-sgRNA plasmid was constructed utilizing the Basic Seamless Cloning and Assembly kit with the primers outlined in Table S5. The existing pCas9-sgRNA plasmid (Addgene, #54,467) was employed as a template, and three fragments were amplified using three pairs of

primers, namely Amp-F/Cas9-R, CAS9-F/sgrNA-F, and xx sgrNA-F (where xx represents the Gene ID)/Amp-R (Table S5). For gene tagging, the gene of interest in the screening was targeted downstream of the translational stop code (sgRNA 3'). The primers comprising the specific sgRNA (CAS9-sgRNA xx) were listed in Table S5 for individual genes. The production of *T. gondii* (Table S3) adhered to the tagging strategy developed in prior studies [18] and depicted in the corresponding figures. The short homology regions targeting the stop codon area were selected before the stop codon (HR3) and downstream of the sgRNA 3' (HR4). The primers possessing HR3 and HR4 were designated as L and T for their specific genes. The amplicon was carried out from the generic tagging plasmid, that is, pLinker-TurboID-4Ty-DHFR, pLinker-6Ty-DHFR, pLinker-6HA-HX, and pLinker-mAID-6Ty-DHFR, which contains TurboID or epitope tags for tagging either at the stop codon region utilizing the corresponding primer pairs (L and T). The CAS9-sgRNA plasmid and the corresponding amplicon with specific homology regions were combined and transfected into recipient lines. The lines were chosen by the corresponding drugs and evaluated by indirect fluorescent assay (IFA).

Transfection and selection of genetically modified lines

Approximately 1×10^7 freshly emerged tachyzoites were combined with the pCAS9-sgRNA plasmid (20–50 μ g) and the corresponding amplicon (2–5 μ g) using 250 μ L of CytoMix buffer in a BTX cuvette with a 4-mm gap. The mixture was then transfected employing a BTX ECM 830 electroporator, a product of Harvard Apparatus. Thereafter, the parasites were cultivated in HFF monolayers, with drugs being added the following day for selection, using the appropriate concentrations of mycophenolic acid (MPA) (25 μ g/mL) and 6-xanthine (6Xa) (50 μ g/mL), or pyrimethamine (Pyri) (3 μ M). Once the selection process had stabilized, which occurred several days later, the selection pools were sub-cloned onto HFF cells in 96-well plates to allow for additional screening.

Indirect Fluorescent Assay (IFA)

Parasites cultivated in HFF layers on coverslips were fixed by utilizing a 4% solution of paraformaldehyde in PBS and underwent permeabilization in PBS that contained 2.5% Bovine Serum Albumin (BSA) and 0.25% Triton X-100. This was followed by incubating the parasites with a variety of primary antibody combinations, then with suitable secondary antibodies conjugated with Alexa Flour IgG-488 or -568. After 3–5 wash cycles with a PBS solution containing 2.5% BSA and 0.05% Tween-20, the coverslips were prepared with ProLong Antifade Mountant, with or without DAPI, after which the parasites were

visualized using a Nikon Ni-E microscope C2+, fitted with a DS-Ri2 Microscope Camera. The colocalization study was conducted employing the NIS Element AR software which was directly interfaced with the confocal system's computer.

Western blotting

Parasites, whether freshly egressed or mechanically produced, were collected and resuspended in PBS combined with 5× Laemmli sample buffer. Subsequently, the proteins were differentiated through the process of SDS-PAGE, which then proceeded to blotting performed by a Bio-Rad wet-blotting system. The execution of Western blots carried out with the aid of fitting primary antibodies merged with LI-COR 800CW or 680CW reagents, or alternatively, streptavidin LI-COR 800CW for the detection of proteins that have been biotinylated. The membranes' visualization was accomplished via the utilization of a Bio-Rad ChemiDOC MP imaging system.

TurboID and biotinylated proteins

The SFA2-TurboID line was grown on HFF monolayers for 24 h and subsequently incubated with 500 μM D-biotin for 90 min. The parasites were fixed with a 4% paraformaldehyde solution for IFA or harvested for Western Blot. IFA and Western Blot were performed with appropriate streptavidin reagents to visualize biotinylated proteins in parasites. The parental line and SFA2-TurboID line was grown in HFF cells for 36 h, followed by the labeling of proteins by 500 μM D-biotin for 90 min, and harvesting of the parasites for purification of biotinylated proteins. In parallel, the SFA2-TurboID parasite after 36 h of growth was harvested, and extracellular parasites were incubated with 500 μM D-biotin for 90 min, followed by a collection of parasites for purification of biotinylated proteins. The parasites were lysed in the buffer containing 1% Triton X-100, 0.2% SDS and 0.5% deoxycholate, and sonicated with a microtip in 550 sonic dismembrators (Thermo-Fisher Scientific). Biotinylated proteins in cleared supernatant were purified using streptavidin magnetic beads, exactly following the protocol described before [43]. The SFA2-TurboID strain was cultivated on HFF substrate layers for a duration of 24 h, after which, they were exposed to a concentration of 500 μM D-biotin for 90 min. The parasites were then subjected to stabilization using a 4% paraformaldehyde compound, following which they were prepared for either IFA or Western Blotting. IFA and Western Blotting procedures were conducted using pertinent streptavidin substances in order to visualize biotinylated proteins present in the parasites. Both the initial strain and the SFA2-TurboID strains were nurtured in HFF cells for a stretch of 36 h. This

period was followed by protein labeling using 500 μM D-biotin for a timeframe of 90 min. After this procedure, the parasites were compiled for the purification of their biotinylated proteins.

Simultaneously, the SFA2-TurboID parasites were gathered after spending 36 h on growth. Extracellular parasites were subjected to exposure to 500 μM D-biotin for a timeframe of 90 min, following which the parasites were assembled for the purification of their biotinylated proteins. Once assembled, the parasites were dispersed in a medium containing 1% Triton X-100, 0.2% SDS, and 0.5% deoxycholate, thereafter undergoing sonication with a microtip in 550 sonic dismembrators; a process facilitated by Thermo-Fisher Scientific. The biotinylated proteins in the precipitated supernatant were subsequently purified utilizing streptavidin magnetic beads, adhering strictly to the protocol outlined previously [43].

Proteomic analysis

The purified biotinylated proteins were separated on SDS-PAGE and stained by Coomassie blue R250, 45% methanol and 10% glacial acetic acid, subsequently dried on SDS-PAGE slice by vacuum. The dried gels were rehydrated, alkylated and washed to remove the stain and SDS, and subjected to steps of mass-spectrometry analysis described as our previous study [41]. The control line RHΔku80Δhxpprt and TurboID fusion lines were analyzed in parallel with two technical replicates. The obtained spectra were searched against the jointed database including human proteins, *T. gondii* (<http://ToxoDB.org>, release 53) and a decoy database by Mascot and Scaffold softwares. The current views in Scaffold were exported into an excel spreadsheet using the following settings of peptide 2, protein threshold 99% and peptide threshold 95%. The resulting data containing both fold change of peptide numbers and *P* value was used to identify the differentially expressed proteins (DEPs). Combined to the phenotypic score, the candidate putative DEPs were retrieved for subsequent functional assays. The biotinylated proteins that had been purified were separated using SDS-PAGE and dyed with Coomassie Blue R250, a mixture of 45% methanol, and 10% glacial acetic acid. They were then dried on an SDS-PAGE slice using a vacuum. Following this, the dried gels were rehydrated, alkylated, and rinsed to eliminate the dye and SDS. These were then subjected to the stages of mass-spectrometry analysis, as delineated in our preceding study [41]. Both the control line RHΔku80Δhxpprt and TurboID fusion lines were examined concurrently, with two technical duplicates. The resulting spectra were examined against a combined database containing human proteins, *T. gondii* (<http://ToxoDB.org>, release 53), and a decoy database using both Mascot and Scaffold

software. The prevailing visualizations in Scaffold were extracted into an excel file using the peptide 2, 99% protein threshold, and 95% peptide threshold settings. The resulting data containing both fold change of peptide numbers and *P* value was used to identify the differentially expressed proteins (DEPs). Combined to the phenotypic score, the candidate putative DEPs were retrieved for subsequent functional assays.

Plaque formation

Parasites freshly lysed were cultivated on HFF cells contained in 6-well plates supplemented with either an inducer (2 μ M 5-Ph-IAA) or standalone ethanol (0.1%) within D5 media at 37 °C for a duration of 7 days. Subsequently, both the host cell monolayers and the parasites were secured in 75% ethanol for a 20-min interval, thereafter undergoing a staining process with 0.5% crystal violet for a minimum of 30 min. The plates underwent sequential washing, were dried at ambient temperature, and had their content scanned using the HP-Scanjet G4050. Use Adobe Photoshop (v16.1.2.355) to crop the image and use ImageJ to analyze the image data.

Parasite replication

The mAID lines derived from TIR1^{F74G} were cultivated on monolayers in 24-well plate setups with coverslips using 2 μ M 5-Ph-IAA for 24 h. The parasites underwent a fixing process with 4% paraformaldehyde for a set duration of 10 min. This was succeeded by blockage and permeabilization utilizing 0.25% Triton X-100 in a PBS setup that contained 2.5% BSA. Afterward, the parasites were subjected to an incubation process with a GAP45 antibody paired with secondary anti-rabbit antibodies which were attached to Alexa Fluor 488. Following the attachment of the coverslips, the samples were visualized using a Nikon Ni-E microscopic tool. Three independent experiments were conducted where unassociated individuals assessed vacuoles containing various quantities of parasites against the identical imagery. Finally, the ratios of vacuoles housing different amounts of parasites were marked against the overall vacuoles examined.

Parasite growth in mice

Mice were randomly divided into groups, with each mouse intraperitoneally injected with 100 parasites. Following this, mice ($n=5$ from each group) were given oral treatment with or without 5-Ph-IAA, and an intraperitoneal injection daily. Their drinking water was a sterile mix containing 1 mg/mL 5-Ph-IAA, 3 mM NaOH, and 5% w/v sucrose, stirred with 2 mg/mL TANG (Mondeléz International), with a final pH of 8.0. At the same time,

each mouse received a daily intraperitoneal injection of a 0.2 mL sterile solution that included 5 mg/mL 5-Ph-IAA and 1 M NaOH, with a pH of 7.8. Control mice were those infected with the TIR1^{F74G} line (+), which received the same 5-Ph-IAA-containing solution in their drinking water and intraperitoneal injection as the mAID line (+) did. Mice's weights and health statuses were recorded everyday until the 17th day.

Phylogenetic analysis

For the phylogenetic analysis, amino acid sequences from them were utilized as queries against a tailored database retrieved from the NCBI-NR database. This used the iterative version of the profile hidden Markov models (HMMs) search system also known as jackhammer (E-values beneath e^{-7}). The taxonomy of this personalized database included classifications such as chlorophyta, streptophyta, rhodophyta, cryptophyta, haptophyta, amoebozoa, fungi, metazoan, and the SAR supergroup. The optimal hit was picked and protein sequences from it were aligned applying Mafft (v7.490) using the L-INS-I algorithm. Regions that were poorly conserved or incorrect were removed automatically using the trimAL software (v1.2.rev57; <https://vicfero.github.io/trimal/>) with the parameter "automated1". Eventually, the resulting tree of the maximum likelihood was constructed by the FastTree software (v2.1) employing the Le-Gascuel (LG) model, and subsequently annotated and displayed via the Chiplot online portal (v1.8.0; <https://www.chiplot.online/>).

Statistics

Statistical analyses were performed using the GraphPad Prism software (version 8.0). Data adhering to a normal distribution pattern were examined by either one-way or two-way ANOVA coupled with Tukey's post-hoc test. For data sets of smaller sizes, the Student's *t*-test was applied. *P*-value of less than 0.05 was deemed statistically significant. Specific statistical details pertaining to the experiments were furnished in the captions provided beneath the figures.

Abbreviations

SFA	Striated fiber assemblin
PV	Parasitophorous vacuole
IMC	Inner membrane complex
S-phase	Synthesis phase
SPF	Specific pathogen-free
MPA	Mycophenolic acid
6Xa	6-Xanthine
Pyri	Pyrimethamine
BSA	Bovine serum albumin
DEP	Differentially expressed protein
HMM	Hidden markov model

Supplementary Information

The online version contains supplementary material available at <https://doi.org/10.1186/s44280-024-00043-1>.

Additional file 1: Table S1. The differential analysis of proteome between RH and SFA2 TurboID strains.

Additional file 2: Table S2. The results of homologous comparison for three SFA proteins.

Additional file 3: Fig. S1. Localization of three candidate proteins in comparison with SFA2-Ty.

Additional file 4: Fig. S2. Phylogenetic analysis of SFA proteins.

Additional file 5: Table S3. Lines used in this study.

Additional file 6: Table S4. Plasmids used in this study.

Additional file 7: Table S5. Primers used in this study.

Authors' contributions

S.L. provided the conception and funding acquisition; Y.L. designed the work, collected, analyzed, interpreted the data, and drafted the manuscript; K.H. contributed in writing, analyzed the data and revised the manuscript; X.T. designed the work, acquisition and analysis; H.D. and H.-Y.D. contributed to the conception and reviewed the work. X.-T.W., X.-W.C. and R.-B.W. provided some advices to design experiments. Q.-Q.W. and M.T.A. reviewed the manuscript. All authors read and approved the final manuscript.

Funding

This work was funded by the National Key Research and Development Project of China (Grant Nos. 2022YFD1800200).

Availability of data and materials

The datasets that support the conclusions of this article are incorporated within the article itself and also in the supplementary files.

Declarations

Ethics approval and consent to participate

In this study, the mouse experiments were conducted according to the guidelines and regulations issued by the Veterinary Office of the China Agricultural University (Issue No. AW11402202-2-1).

Consent for publication

The data presented in this manuscript have not been previously reported by the authors nor are they under consideration for publication elsewhere. All authors have contributed to, reviewed, and approved the final, submitted version of the manuscript.

Competing interests

All authors declare that they have no competing interests.

Received: 10 January 2024 Revised: 20 February 2024 Accepted: 11 March 2024

Published online: 13 May 2024

References

- Sibley LD. Intracellular parasite invasion strategies. *Science*. 2004;304(5668):248–53.
- Deganich M, Boudreaux C, Benmerzouga I. Toxoplasmosis infection during pregnancy. *Trop Med Infect Dis*. 2022;8(1):3.
- Damar CT, Can IN, Deniz M, Torun A, Akcabay C, Guzelcicek A. Toxoplasmosis: a timeless challenge for pregnancy. *Trop Med Infect Dis*. 2023;8(1):63.
- Almallah TM, Khedr SI, El Nouby KA, Younis SS, Elazeem MA, Elmehy DA. The synergetic potential of *Lactobacillus delbrueckii* and *Lactobacillus fermentum* probiotics in alleviating the outcome of acute toxoplasmosis in mice. *Parasitol Res*. 2023;122(4):927–37.
- Zafar A, Khan MK, Abbas RZ, Saqib M, Javed H. Molecular evidence of toxoplasmosis in people living with HIV in Pakistan. *Int J STD Aids*. 2023;34(5):346–52.
- Gubbels MJ, White M, Szatanek T. The cell cycle and *Toxoplasma gondii* cell division: tightly knit or loosely stitched? *Int J Parasitol*. 2008;38(12):1343–58.
- Engelberg K, Bechtel T, Michaud C, Weerapana E, Gubbels MJ. Proteomic characterization of the *Toxoplasma gondii* cytokinesis machinery portrays an expanded hierarchy of its assembly and function. *Nat Commun*. 2022;13(1):4644.
- White MW, Suvorova ES. Apicomplexa cell cycles: something old, borrowed, lost, and new. *Trends Parasitol*. 2018;34(11):759–771.
- Ferguson DJ, Hutchison WM, Dunachie JF, Siim JC. Ultrastructural study of early stages of asexual multiplication and microgametogony of *Toxoplasma gondii* in the small intestine of the cat. *Acta Pathol Microbiol Scand B Microbiol Immunol*. 1974;82(2):167–81.
- Lechtreck KF. Striated fiber assemblin in apicomplexan parasites. *Mol Biochem Parasit*. 2003;128(1):95–9.
- Radke JR, Striemen B, Guerin MN, Jerome ME, Roos DS, White MW. Defining the cell cycle for the tachyzoite stage of *Toxoplasma gondii*. *Mol Biochem Parasitol*. 2001;115(2):165–75.
- Chen AL, Kim EW, Toh JY, Vashisht AA, Rashoff AQ, Van C, et al. Novel components of the *Toxoplasma* inner membrane complex revealed by BioID. *Mbio*. 2015;6(1):10–1128.
- Li MZ, Liu J, Wu YY, Wu YH, Sun XD, Fu Y, et al. Requirement of *Toxoplasma gondii* metacaspases for IMC1 maturation, endodyogeny and virulence in mice. *Parasite Vector*. 2021;14(1):400.
- Marshall WF. Basal bodies: platforms for building cilia. *Curr Top Dev Biol*. 2008;85:1–22.
- Francia ME, Jordan CN, Patel JD, Sheiner L, Demerly JL, Fellows JD, et al. Cell division in Apicomplexan parasites is organized by a homolog of the striated rootlet fiber of algal flagella. *PLoS Biol*. 2012;10(12):e1001444.
- Long S, Brown KM, Drewry LL, Anthony B, Phan IQH, Sibley LD. Calmodulin-like proteins localized to the conoid regulate motility and cell invasion by *Toxoplasma gondii*. *PLoS Pathog*. 2017;13(5):e1006379.
- Hu K, Johnson J, Florens L, Fraunholz M, Suravajjala S, DiLullo C, et al. Cytoskeletal components of an invasion machine—the apical complex of *Toxoplasma gondii*. *PLoS Pathog*. 2006;2(2):e13.
- Long S, Anthony B, Drewry LL, Sibley LD. A conserved ankyrin repeat-containing protein regulates conoid stability, motility and cell invasion in *Toxoplasma gondii*. *Nat Commun*. 2017;8(1):2236.
- Behnke MS, Wootton JC, Lehmann MM, Radke JB, Lucas O, Nawas J, et al. Coordinated progression through two subtranscriptomes underlies the tachyzoite cycle of *Toxoplasma gondii*. *PLoS ONE*. 2010;5(8):e12354.
- Brown KM, Long S, Sibley LD. Plasma membrane association by N-acylation governs PKG function in *Toxoplasma gondii*. *mBio*. 2017;8(3):3.
- Yesbolatova A, Saito Y, Kitamoto N, Makino-Itou H, Ajima R, Nakano R, et al. The auxin-inducible degron 2 technology provides sharp degradation control in yeast, mammalian cells, and mice. *Nat Commun*. 2020;11(1):5701.
- Lechtreck KF, Melkonian M. Striated microtubule-associated fibers: identification of assemblin, a novel 34-kD protein that forms paracrystals of 2-nm filaments in vitro. *J Cell Biol*. 1991;115(3):705–16.
- Weber K, Geisler N, Plessmann U, Bremerich A, Lechtreck KF, Melkonian M. SF-assemblin, the structural protein of the 2-nm filaments from striated microtubule associated fibers of algal flagellar roots, forms a segmented coiled coil. *J Cell Biol*. 1993;121(4):837–45.
- Dutcher SK. Elucidation of basal body and centriole functions in *Chlamydomonas reinhardtii*. *Traffic*. 2003;4(7):443–51.
- Fox BA, Ristuccia JG, Gigley JP, Bzik DJ. Efficient gene replacements in *Toxoplasma gondii* strains deficient for nonhomologous end joining. *Eukaryot Cell*. 2009;8(4):520–9.
- Huynh MH, Carruthers VB. Tagging of endogenous genes in a *Toxoplasma gondii* strain lacking Ku80. *Eukaryot Cell*. 2009;8(4):530–9.
- Goldstein RE. Green Algae as model organisms for biological fluid dynamics. *Annu Rev Fluid Mech*. 2015;47:343–75.
- Machemer H. Ciliary activity and the origin of metachrony in Paramecium: effects of increased viscosity. *J Exp Biol*. 1972;57(1):239–59.

29. Lechtreck KF, Melkonian M. SF-assemblin, striated fibers, and segmented coiled coil proteins. *Cell Motil Cytoskeleton*. 1998;41(4):289–96.
30. Yang J, Liu X, Yue G, Adamian M, Bulgakov O, Li T. Rootletin, a novel coiled-coil protein, is a structural component of the ciliary rootlet. *J Cell Biol*. 2002;159(3):431–40.
31. Priyanka PP, Yenugu S. Coiled-Coil Domain-Containing (CCDC) proteins: functional roles in general and male reproductive physiology. *Reprod Sci*. 2021;28(10):2725–34.
32. Park WM. Coiled-coils: the molecular zippers that self-assemble protein nanostructures. *Int J Mol Sci*. 2020;21(10):3584.
33. Craven SJ, Condon SGF, Diaz Vazquez G, Cui Q, Senes A. The coiled-coil domain of *Escherichia coli* FtsLB is a structurally detuned element critical for modulating its activation in bacterial cell division. *J Biol Chem*. 2022;298(1):101460.
34. Kantsadi AL, Hatzopoulos GN, Gonczy P, Vakonakis I. Structures of SAS-6 coiled coil hold implications for the polarity of the centriolar cartwheel. *Structure*. 2022;30(5):671–84.
35. Mason JM, Arndt KM. Coiled coil domains: stability, specificity, and biological implications. *ChemBioChem*. 2004;5(2):170–6.
36. Truebestein L, Leonard TA. Coiled-coils: the long and short of it. *BioEssays*. 2016;38(9):903–16.
37. Rahmani H, Ma W, Hu Z, Daneshparvar N, Taylor DW, McCammon JA, et al. The myosin II coiled-coil domain atomic structure in its native environment. *Proc Natl Acad Sci U S A*. 2021;118(14):e2024151118.
38. Gubbels MJ, Coppens I, Zarringhalam K, Duraisingh MT, Engelberg K. The modular circuitry of apicomplexan cell division plasticity. *Front Cell Infect Microbiol*. 2021;11:670049.
39. Gubbels MJ, Keroack CD, Dangoudoubiyam S, Worliczek HL, Paul AS, Bauwens C, et al. Fussing about fission: defining variety among mainstream and exotic apicomplexan cell division modes. *Front Cell Infect Microbiol*. 2020;10:269.
40. Sheffield HG, Melton ML. The fine structure and reproduction of *Toxoplasma gondii*. *J Parasitol*. 1968;54(2):209–26.
41. Wan W, Dong H, Lai DH, Yang J, He K, Tang X, et al. The *Toxoplasma* micropore mediates endocytosis for selective nutrient salvage from host cell compartments. *Nat Commun*. 2023;14(1):977.
42. Wang QQ, Sun M, Tang T, Lai DH, Liu J, Maity S, et al. Functional screening reveals *Toxoplasma* prenylated proteins required for endocytic trafficking and rhoptry protein sorting. *mBio*. 2023;14(4):e0130923.
43. Long S, Brown KM, Sibley LD. CRISPR-mediated tagging with BirA allows proximity labeling in *Toxoplasma gondii*. *Bio Protoc*. 2018;8(6):e2768.

Publisher's Note

Springer Nature remains neutral with regard to jurisdictional claims in published maps and institutional affiliations.